Absorption and scattering effects of Maalox, chlorophyll, and sea salt on a micro-LED-based underwater wireless optical communication [Invited]

Pengfei Tian (田朋飞)[1,*,†], Honglan Chen (陈红兰)[1,†], Peiyao Wang (王培瑶)[1], Xiaoyan Liu (刘晓艳)[1], Xinwei Chen (陈新伟)[1], Gufan Zhou (周顾帆)[1], Shuailong Zhang (张帅龙)[2], Jie Lu (鲁 杰)[1], Pengjiang Qiu (仇鹏江)[1], Zeyuan Qian (钱泽渊)[1], Xiaolin Zhou (周小林)[1], Zhilai Fang (方志来)[1], Lirong Zheng (郑立荣)[1], Ran Liu (刘 冉)[1], and Xugao Cui (崔旭高)[1,]**

[1]*Institute for Electric Light Sources, School of Information Science and Technology, Engineering Research Center of Advanced Lighting Technology, and Academy of Engineering and Technology, Fudan University, Shanghai 200433, China*

[2]*Department of Chemistry, University of Toronto, Toronto, Ontario M5S 3H6, Canada*

**Corresponding author: pftian@fudan.edu.cn; **corresponding author: cuixugao@fudan.edu.cn*

Received August 25, 2019; accepted September 12, 2019; posted online October 14, 2019

In this work, a blue gallium nitride (GaN) micro-light-emitting-diode (micro-LED)-based underwater wireless optical communication (UWOC) system was built, and UWOCs with varied Maalox, chlorophyll, and sea salt concentrations were studied. Data transmission performance of the UWOC and the influence of light attenuation were investigated systematically. Maximum data transmission rates at the distance of 2.3 m were 933, 800, 910, and 790 Mbps for experimental conditions with no impurity, 200.48 mg/m^3 Maalox, 12.07 mg/m^3 chlorophyll, and 5 kg/m^3 sea salt, respectively, much higher than previously reported systems with commercial LEDs. It was found that increasing chlorophyll, Maalox, and sea salt concentrations in water resulted in an increase of light attenuation, which led to the performance degradation of the UWOC. Further analysis suggests two light attenuation mechanisms, e.g., absorption by chlorophyll and scattering by Maalox, are responsible for the decrease of maximum data rates and the increase of bit error rates. Based on the absorption and scattering models, excellent fitting to the experimental attenuation coefficient can be achieved, and light attenuation by absorption and scattering at different wavelengths was also investigated. We believe this work is instructive apply UWOC for practical applications.

OCIS codes: 220.4830, 290.5850, 290.5825, 230.6080.
doi: 10.3788/COL201917.100010.

Underwater wireless optical communication (UWOC) has attracted a lot of research interest due to its advantages of high data transmission rate, low latency, high security, and low cost when compared with traditional underwater acoustic communication[1–5]. UWOC can be potentially applied to oceanography researches, ocean circulation monitoring, offshore oil exploration, sea floor survey, and pollution detection[1–8].

In general, performances of a UWOC system are mainly determined by light sources (transmitters), channel conditions, photodetectors (receivers), modulation schemes, and other units. Laser diodes (LDs)[3,4,6,8] and light-emitting diodes (LEDs)[7,9,10] are normally used as light sources for UWOC, and UWOC links with LDs have demonstrated high data transmission rates. The highest data transmission rate of LDs for UWOC is 25 Gbps, as reported by Li *et al.*[11]. However, LDs are expensive and not safe to human eyes[1,2]. Commercial LEDs are cheap and convenient but suffer from low modulation bandwidths for data communication. Recently, the micro-LED has been demonstrated as a novel light source for high-speed optical communication due to its advantage of high modulation bandwidth[1,12–14]. However, practical applications of micro-LED-based UWOC are still limited by the optical absorption and scattering due to the complex underwater channel, the requirement of highly precise alignment conditions of optical transceivers, and the requirement of reliable underwater devices, including efficient device power consumption and reliable device batteries[1,2].

In practical cases, especially in seawater, UWOC channels are highly sensible to phytoplankton, nonchlorophyllous particles, yellow substances, and turbulence[10,15], where light can be scattered and/or absorbed. In water with suspension particles, e.g., Maalox consisting of $Al(OH)_3$ and $Mg(OH)_2$ particles, scattering occurs in the process where the light interacts with particles and gets scattered to different directions[3]. Although in pure water, absorption is usually a single interaction between light and matter, it was reported that in chlorophyll-added water both absorption by light at long wavelengths and scattering by light at short wavelengths could make a difference[16,17]. Therefore, there exist different interactions between light and matter, leading to different cases of light attenuation in water, which influences the performance of UWOC. Recently, there are several theoretical studies about scattering and absorption effects on UWOC[18,19]. However, the influence of chlorophyll on the performances of micro-LED-based UWOC has been rarely reported in previous literatures. Experimental studies on light propagation properties of micro-LED-based UWOC are not adequate yet.

Here, we propose a high-bandwidth micro-LED-based UWOC system in water with different concentrations of Maalox, chlorophyll, and sea salt. Seawater environments with different impurities were simulated and light attenuation mechanisms due to absorption and scattering were theoretically and experimentally studied. The highest data rate of our micro-LED-based UWOC with an on–off keying (OOK) modulation scheme is 933 Mbps, which is much higher than that of normal LED-based UWOC. In addition, our study provides a simple approach of using only one substance, e.g., Maalox, to simulate attenuation coefficients, same as those of the different water types in real sea water, which helps future studies of UWOC in practical scenarios. Our Letter is organized as follows. Firstly, we introduce micro-LED-based UWOC and the attenuation effect in the UWOC system. Then, light absorption and scattering theories in water are discussed. The following part is about the experimental setup, results, and discussion, including micro-LED characteristics, UWOC under diluted Maalox suspension, diluted chlorophyll solution, and sea salt solution, and wavelength-dependent optical transmission spectra.

In UWOC systems, light absorption and scattering due to water molecules, suspension particles, chlorophyll, dissolved salt, and other impurities are proposed to be the main mechanisms for light attenuation[2,16,17,20–22]. To confirm the mechanisms and clarify the ambiguity, we discuss relevant models, then establish our UWOC links, and verify them experimentally in different experimental conditions.

To quantitatively characterize the light attenuation, the transmitted and received optical powers of the light beam are determined by the Beer–Lambert law[2,6,20]:

$$\frac{P_R}{P_T} = e^{-cx}, \tag{1}$$

where P_R and P_T represent the detected transmitted and received optical powers of the light beam, c is the attenuation coefficient with the unit meters to the negative power (m^{-1}), and x is the underwater channel distance, which is 2.3 m in this experiment. Based on Eq. (1), we can extract the attenuation coefficient by the following equation:

$$c = -\frac{\ln \frac{P_R}{P_T}}{x}. \tag{2}$$

The absorption coefficient of chlorophyll a_c can be expressed as a power function of chlorophyll concentration[15,23]:

$$a_c(\lambda) = 0.06A(\lambda) \cdot \left(\frac{\mathrm{Chl}_a}{\mathrm{Chl}_0}\right)^{\alpha}, \tag{3}$$

where Chl_0 represents a constant of 1 $\mathrm{mg/m^3}$, Chl_a represents the concentration of chlorophyll, $A(\lambda)$ represents the chlorophyll spectral absorption spectrum at a specific reference concentration, which is 0.971 at the wavelength of 445 nm, and α represents a constant[15,23].

The suspension particles responsible for the scattering effects can be divided into different kinds (small particles or large particles) to build the scattering model[23,24]. The empirical formulas for the scattering coefficients of small and large particles can be expressed as[15,23]

$$b_S(\lambda) = 1.151302\left(\frac{400}{\lambda}\right)^{1.7}, \tag{4}$$

and

$$b_L(\lambda) = 0.341074\left(\frac{400}{\lambda}\right)^{0.3}, \tag{5}$$

respectively, where b_S ($\mathrm{m^2/g}$) and b_L ($\mathrm{m^2/g}$) are scattering coefficients of small and large particles, respectively, and λ is the wavelength of light with the unit of nanometers (nm). The scattering coefficient of particles can be calculated as

$$b_p(\lambda) = b_S \times C_S + b_L \times C_L, \tag{6}$$

where C_S and C_L represent concentrations of small particles and large particles, respectively. Based on Eqs. (1)–(6), we performed fittings to attenuation coefficients for our UWOC system with different impurity concentrations.

To study the absorption and scattering effects in different water conditions experimentally, our UWOC system was set up, as shown in Fig. 1(a). On the transmitter side, pseudo-random binary sequences (PRBSs) generated by a pulse pattern generator module (0.1–14 Gbps) from a signal quality analyzer (Anritsu MP1800) were combined with a direct current (DC) generated by a Yokogawa source (GS610) to drive a blue micro-LED through a bias tee (Mini-circuits ZFBT-6GW+). The non-return-to-zero (NRZ) OOK modulation scheme was used. The packaged micro-LED transmitter is shown in Fig. 1(b). After being collimated by a non-spherical lens, the blue light from the micro-LED in Fig. 1(a) was transmitted through a 2.3 m long water tank. Different concentrations of Maalox, chlorophyll, and sea salt were used to achieve different water conditions [see Figs. 1(c)–1(f)]. The artificial sea salt used in this work mainly contains sodium chloride (NaCl) and a small proportion of other elements including magnesium (Mg), potassium (K), calcium (Ca), sulfate, strontium (Sr), and bicarbonate. Maalox suspension mainly consists of $\mathrm{Al(OH)_3}$ (195 mg/5 mL) and $\mathrm{Mg(OH)_2}$ (220 mg/5 mL). The main constitute of the Swisse chlorophyll is sodium magnesium chlorophyllin (20 mg/mL), together with a certain proportion of purified water, K, and Na. On the receiver side, the transmitted light beams were focused by a Fresnel lens, whose focal length and diameter are both 10 cm. A high-bandwidth avalanche photodiode (APD, Thorlabs, APD210, 1 GHz) or a

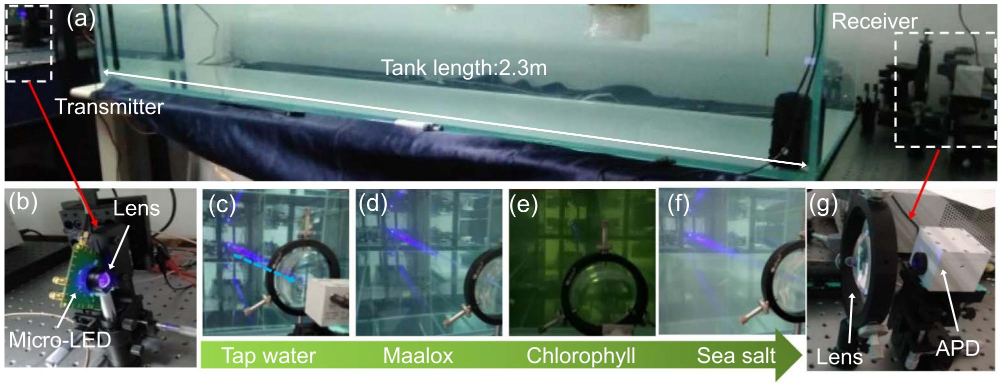

Fig. 1. Images of (a) the transmission link, (b) the packaged micro-LED transmitter, the light beam through (c) tap water, (d) 100.24 mg/m^3 Maalox, (e) 1207.73 mg/m^3 chlorophyll, and (f) 5 kg/m^3 sea salt solutions, and (g) the APD receiver.

high-sensitivity APD (Hamamatsu, APD12702, 100 MHz) was used to detect the optical signal in Fig. 1(g). The light output power was measured at the receiver with an optical power meter. Bit error rate (BER) was tested by an error detector module inside the signal quality analyzer. An oscilloscope (Agilent 86100A, 14 GHz bandwidth) was used to record eye diagrams. The transmission spectrum was measured with a spectrometer covering the ultra-violet and visible spectrum (LengGuang 759S). Figures 1(c)–1(f) show the images of light beams transmitting through tap water, Maalox (100.24 mg/m^3), chlorophyll (1207.73 mg/m^3), and sea salt (5 kg/m^3) solutions, respectively.

Figure 2(a) shows the *I*-*V* characteristic of the micro-LED. It is clear that the micro-LED can work under high current densities, enabling high modulation bandwidth of ~230 MHz at a current of 35 mA[12,13]. The highest driving current density is around 4375 A/cm^2, which is 43 times as high as that of conventional LEDs[25,26]. Figure 2(b) shows the electroluminescence (EL) spectra under different driving currents of the micro-LED. It can be observed that as the current increased from 1 mA to 70 mA, the EL peaks shifted from ~448 nm to ~439 nm. The carrier screening effect and band filling effect contribute to the blue shift, while the self-heating effect suppresses the blue shift[1]. Light output powers at the receiver with increasing driving currents of the micro-LED in varied concentrations of Maalox-added water are shown in Fig. 2(c). We only measured the received light output power directed by the lens, which was useful for UWOC. It can be found that light output power decreases rapidly with increasing Maalox concentrations, indicating that light was attenuated due to scattering by Maalox in water. In addition, it is observed that light output power increases nonlinearly with a roll off with the driving current, which is due to efficiency droop and thermal effects of GaN-based LEDs[1].

Light scattering in water by non-algae suspended particles can lead to light attenuation, while the effect of light absorption by non-algae suspended particles is usually negligible[27]. The processes and mechanisms of light scattering are quite complicated and vary for different cases. For simplicity, Maalox suspension, mainly consisting of $Al(OH)_3$ (220 mg/5 mL) and $Mg(OH)_2$ (195 mg/5 mL), was usually added in water to simulate the non-algae suspended particles and then to study the light scattering effect in ocean water with suspended particles[2,20].

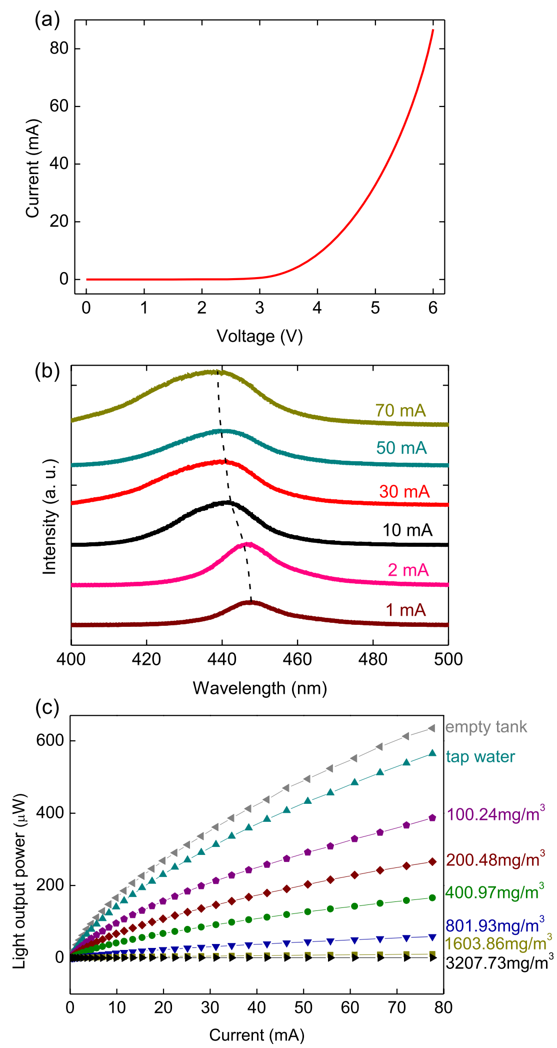

Fig. 2. (a) *I*-*V* characteristic of the micro-LED. (b) The EL spectra under different currents of the micro-LED. (c) Light output powers at the receiving end with increasing driving currents of the micro-LED in varied concentrations of Maalox solution.

Since Maalox contains $Al(OH)_3$ and $Mg(OH)_2$ as the primary ingredients, it can be a simple approach to simulate the particle distribution in certain types of seawater[20]. Moreover, there have been a few previous reports performed on the scattering effect with Maalox[2,20,28]. So, Maalox suspension was chosen as the scattering medium in our work.

We performed UWOC experiments in water with different concentrations of Maalox using a micro-LED at a typical driving current of 34.62 mA. Light attenuation coefficients in water with varieties of Maalox concentrations were calculated by Eq. (2) with data in Fig. 2(c). In our work, an empty water tank was used as a reference, and light output powers at the receiving end after light transmitting through the tank with Maalox-added water and without water were taken as the values of P_R and P_T in Eq. (2), respectively, to minimize the effect of the divergence angle, the large spot, and the reflection. The attenuation results are shown in Fig. 3(a). The attenuation coefficients increase with scaling Maalox concentrations from 100.24 mg/m^3 to 3207.73 mg/m^3. The attenuation coefficients of commonly defined water types, i.e., pure sea water, clear ocean water, coastal ocean water, and turbid harbor water were marked in Fig. 3(a) for comparison[2,17]. From Fig. 3(a), 200.48 mg/m^3 Maalox-added water can approximately simulate coastal ocean water.

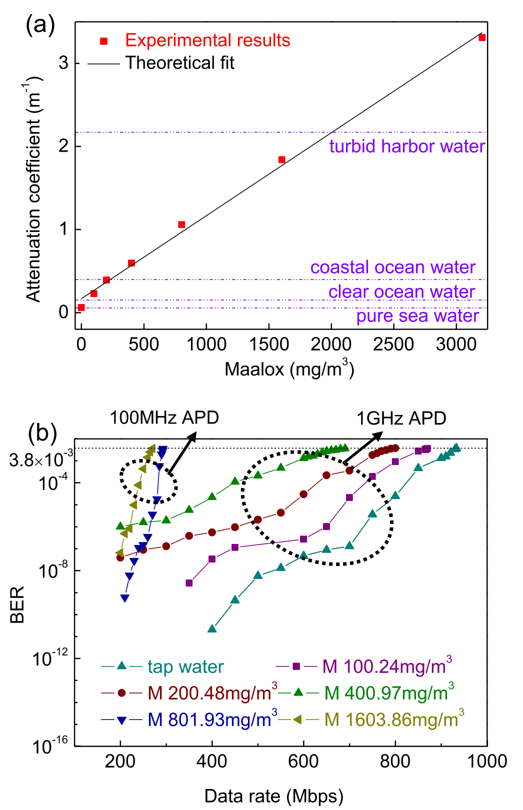

Fig. 3. (a) Experimental attenuation coefficients and the fitting results in water with different Maalox concentrations. The purple dash line shows the attenuation coefficients of four typical water qualities. (b) Variation of BERs with increasing data rates with different Maalox concentrations.

Thus, adding Maalox in the water solution could be a simple approach to achieve different water types for UWOC research.

In our experiment, the typical sizes of $Al(OH)_3$ and $Mg(OH)_2$ particles are tens of micrometers (μm)[28], which belongs to large particles in Eq. (6)[29], and therefore, the attenuation coefficient of Maalox-added water can be fitted by

$$b(\lambda) = c_w(\lambda) + b_M \times C_M, \tag{7}$$

where $c_w(\lambda)$ represents the attenuation coefficient of water at a specific wavelength, and b_M and C_M represent the scattering coefficient and concentration of $Al(OH)_3$ and $Mg(OH)_2$ particles, respectively. The solid line in Fig. 3(a) is a theoretical fit of experimental results of attenuation coefficients with different Maalox concentrations using the linear fitting function, with adjusted R square of 0.995. Although slight deviations of experimental data exist from the fitted line, the good linearity indicates that the scattering effect is dominant for diluted Maalox suspension.

Figure 3(b) shows characteristics of BERs versus data rates. At low Maalox concentrations of 100.24 mg/m^3, 200.48 mg/m^3, and 400.97 mg/m^3, BERs were tested with a high-bandwidth APD (Thorlabs, APD210, 1 GHz). At high Maalox concentrations of 801.93 mg/m^3 and 1603.86 mg/m^3, BERs were tested with a high-sensitivity APD (Hamamatsu, APD12702, 100 MHz), as the signal is too weak for the high-bandwidth APD, which is also the reason why the BERs of UWOC with high Maalox concentrations of 801.93 mg/m^3 and 1603.86 mg/m^3 are lower at the data rates of ~200 Mbps than those with lower Maalox concentrations of 400.97 mg/m^3 and 200.48 mg/m^3. The typical spectral responsivity of the used APD is about 7.5 A/W at the wavelength of 445 nm. The received optical power at the receiver ranges from hundreds of nanowatts (nW) to hundreds of microwatts (μW), higher than the minimum detected power of the APD. From Fig. 3(b), maximum data rates are 933, 870, 800, 690, 293, and 270 Mbps for UWOC with 0 (tap water), 100.24, 200.48, 400.97, 801.93, and 1603.86 mg/m^3 Maalox under a forward error correction (FEC) threshold of 3.8×10^{-3}, respectively. With higher Maalox concentrations, lower maximum data rates of our system were achieved. The maximum data rate of 870 Mbps with 100.24 mg/m^3 Maalox is much higher than that in previous reports using commercial broad-area blue LEDs[9], owing to the higher bandwidth of micro-LEDs in our works.

The data rate versus attenuation of light output power of our UWOC with different concentrations of Maalox at the BER of 3×10^{-3} is shown in Fig. 4. From Fig. 4, it can be found that the data rate decreases from ~927 Mbps to ~267 Mbps as the attenuation increases from 0 dB to −17.77 dB. Initially the data rate decreases slowly as the attenuation increases; for instance, increasing attenuation from −1.68 dB to −3.31 dB only results in 9.13% reduction of data rate from 856.71 to 778.48 Mbps, which

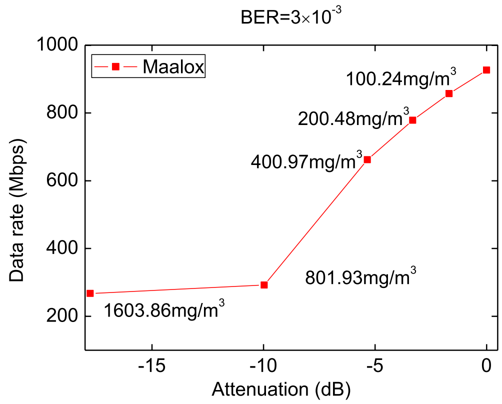

Fig. 4. Data rate versus attenuation of light output power with different Maalox concentrations at the BER of 3×10^{-3}.

demonstrates that besides the light output power, the high bandwidth of micro-LED plays a key role in the high-speed UWOC under OOK modulation. However, when the attenuation is higher than around −5 dB, the data rate drops significantly for the reason that light can hardly propagate through water with high concentrations of Maalox. Furthermore, when the concentration is higher than 801.93 mg/m^3, the decrease of data rate is slowed down, which may be caused by the limited bandwidth of 100 MHz of the high-sensitivity APD. These results are consistent with the variations of the attenuation coefficient in Fig. 3(a) and BERs in Fig. 3(b).

Eye diagrams of the UWOCs are shown in Fig. 5. Figures 5(a) and 5(d) correspond to UWOC with 200.48 mg/m^3 Maalox at data rates of 200 Mbps and 800 Mbps, respectively; Figs. 5(b) and 5(e) correspond to UWOC with 400.97 mg/m^3 Maalox at data rates of 200 Mbps and 690 Mbps, respectively; Figs. 5(c) and 5(f) correspond to UWOC with 1603.86 mg/m^3 Maalox at data rates of 200 Mbps and 270 Mbps, respectively, using a high-sensitivity 100 MHz APD as the receiver. The eyes at the data rate of 200 Mbps under 200.48 mg/m^3, 400.97 mg/m^3, and 1603.86 mg/m^3 Maalox are open and clear, with the corresponding BERs of 3.9×10^{-8}, 1×10^{-6}, and 6.5×10^{-8}, respectively. The relatively lower BERs and the eye diagrams in Figs. 5(a)–5(c) are due to the low data rate. From Figs. 5(d), 5(e), and 5(f), all eyes are nearly closed at maximum data rates of 800, 690, and 270 Mbps for UWOCs with 200.48, 400.97, and 1603.86 mg/m^3 Maalox with the BERs of 3.74×10^{-3}, 3.65×10^{-3}, and 3.64×10^{-3}, respectively. The results in Fig. 5 are consistent with those of BERs in Fig. 3(b). From the analysis above, performances of UWOCs are degraded with increasing concentrations of Maalox.

Sodium magnesium chlorophyllin (Swisse chlorophyll), obtained from natural chlorophyll, is a kind of semisynthetic porphyrins and is soluble in water[30]. Such chlorophyll was adopted to simulate the attenuation effect of sea water with organic particles, phytoplanktons in particular, which can absorb light[16]. The Swisse chlorophyll is different from natural chlorophyll, as both absorption and scattering affect the UWOC for natural chlorophyll[2,16]. In our experiments, we mainly investigated the absorption effects by chlorophyll.

Similarly, we performed UWOC experiments under conditions of varied chlorophyll concentrations in water with micro-LEDs at a typical driving current of 34.62 mA. Light attenuation coefficients were calculated and shown in Fig. 6(a) by red squares. It can be found that the attenuation coefficients of light increase nonlinearly with increasing chlorophyll concentrations in water, which originates from the absorption effects of chlorophyll. The attenuation coefficient of chlorophyll-added water can be expressed as a function of chlorophyll concentration, according to Eq. (3). The parameters are as defined in Eqs. (3) and (7). Equation (8) is a function of optical wavelength λ. We found that the full width at half-maximum (FWHM) of the micro-LED is ∼30 nm at 34.62 mA, and the corresponding transmission percentages are all above 89%, making it possible to choose a

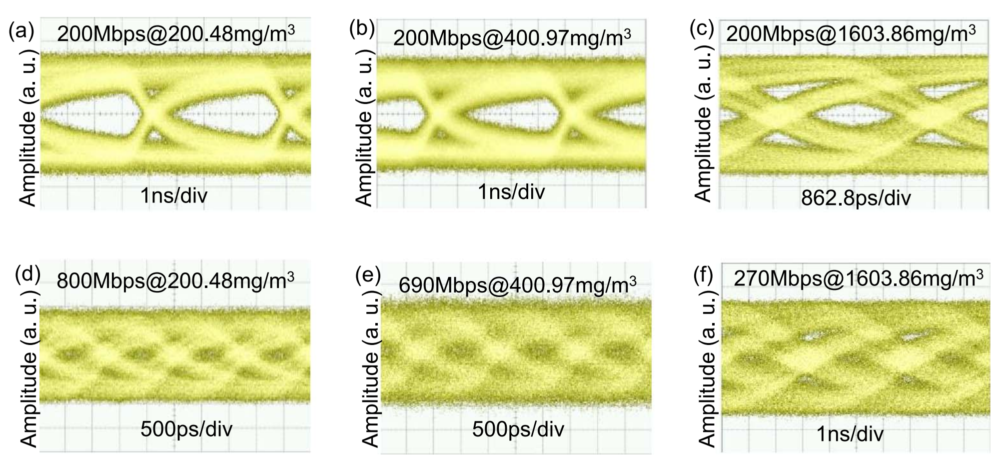

Fig. 5. Eye diagrams at different concentrations of Maalox of (a) 200.48 mg/m^3, (b) 400.97 mg/m^3, and (c) 1603.86 mg/m^3 at a data rate of 200 Mbps, (d) 200.48 mg/m^3 at a data rate of 800 Mbps, (e) 400.97 mg/m^3 at a data rate of 690 Mbps, and (f) 1603.86 mg/m^3 at a data rate of 270 Mbps.

wavelength around the EL peak for approximation. So, we chose the typical wavelength of 445 nm to fit Eq. (8) in this work. The formula could be used to fit the nonlinear increase of the attenuation coefficient with increasing chlorophyll concentration. When α in Eq. (8) is 0.0565, the attenuation coefficient of chlorophyll-added water can be fitted well by Eq. (8), as shown in Fig. 6(a) (solid line), indicating that the absorption effect of chlorophyll plays a leading role in the light attenuation in this work. In addition, the value of α in Eq. (8) differs from previous reports of 0.0602[15,23]. The possible reason is that the scattering effect by chlorophyll in our UWOC system is weak but still available.

$$a(\lambda) = c_w(\lambda) + 0.06A(\lambda) \cdot \left(\frac{\mathrm{Chl}_a}{\mathrm{Chl}_0}\right)^{\alpha}. \tag{8}$$

Variations of BERs with increasing data rates of the UWOC system are presented in Fig. 6(b). When more chlorophyll was added, lower maximum data rates of the UWOC systems were achieved due to the absorption effect of chlorophyll.

Natural sea salt is a mixture of NaCl, $MgCl_2$, $CaSO_4$, $MgSO_4$, Na_2SO_4, and K_2SO_4. In comparison, the artificial sea salt used in this work mainly contains NaCl and a small proportion of other elements, including Mg, K, Ca, sulfate, Sr, and bicarbonate. As shown in Fig. 1(f), although the attenuation of dissolved salt in water could be neglected[21], the sea-salt-added water turns turbid, possibly due to the high concentrations of Ca and Mg ions, as well as the suspended particles of partially undissolved $CaSO_4$, which also contributes to the scattering effect.

UWOC experiments were performed under conditions of varied concentrations of sea-salt-added water with micro-LEDs at a typical driving current of 34.62 mA. Light attenuation coefficients were calculated and shown in Fig. 7(a) by red squares. It can be seen that the attenuation coefficient increases linearly with increasing sea salt concentrations. The concentrations of sea salt were represented with the unit of kilograms per meter cubed (kg/m^3) [1 kg/m^3 = 1 g/kg (salinity)[21]]. We assume that only large particles dominate in the sea salt solution in this experiment. The scattering coefficient at a specific wavelength can be fitted by Eq. (7). The attenuation coefficients of light were fitted, as shown in Fig. 7(a), by a solid line, indicating the dominate role of the scattering effect.

Variations of BERs with increasing data rates of the UWOC with sea-salt-added water are shown in Fig. 7(b). It is observed that maximum data rates decrease with increasing sea salt concentrations, due to the scattering effect of sea salt in water.

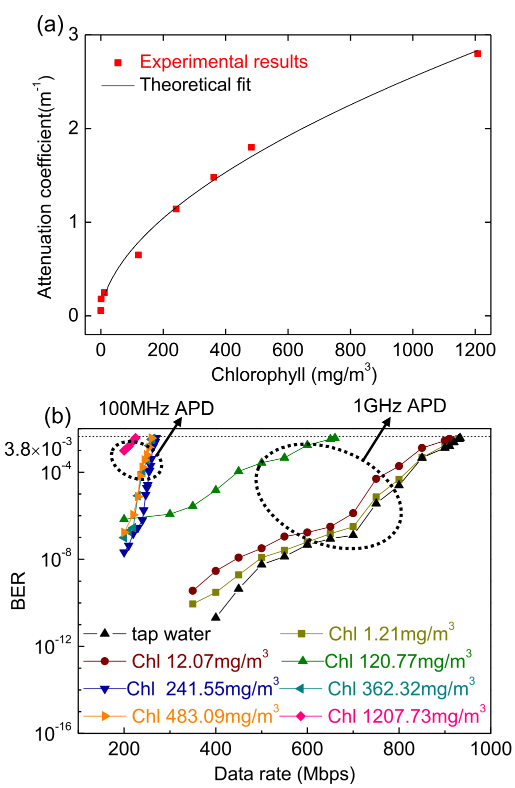

Fig. 6. (a) Experimental attenuation coefficients and the fitting results in water with different chlorophyll concentrations. (b) Variation of BERs with increasing data rates for different chlorophyll concentrations.

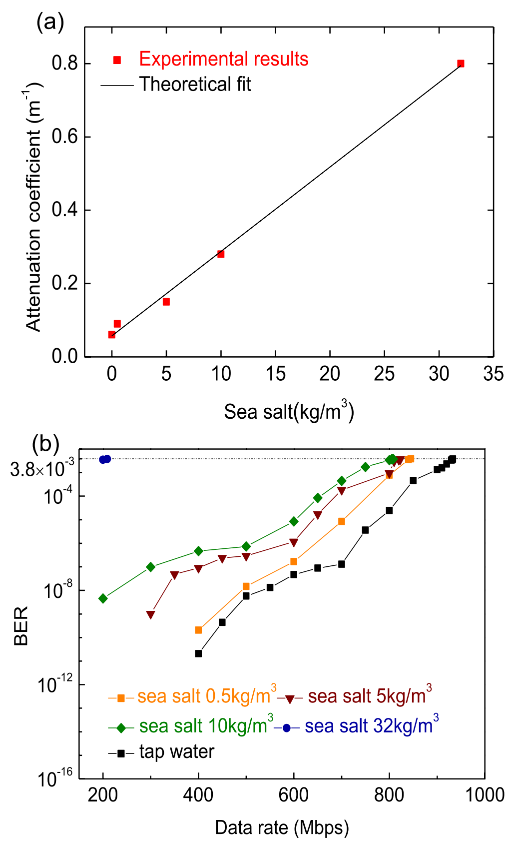

Fig. 7. (a) Experimental attenuation coefficients and the fitting results in water with different sea salt concentrations. (b) Variation of BERs with increasing data rates for different sea salt concentrations, measured by 1 GHz APD.

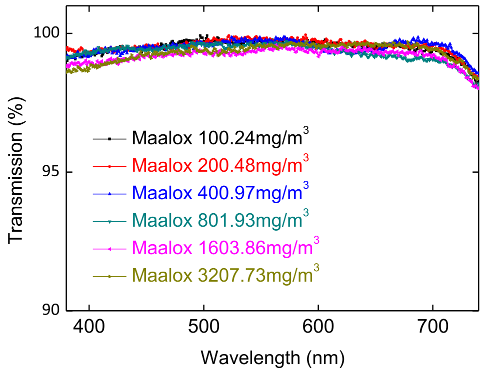

Fig. 8. Transmission spectra of water with different Maalox concentrations.

Furthermore, to predict the wavelength-dependent UWOC under different water qualities, light transmission spectra in the range of 380–740 nm through Maalox-added water are shown in Fig. 8. The spectra were measured by an ultra-violet and visible spectrometer with a 10 mm quartz cuvette. A 5 mm quartz cuvette with the same concentration of the tested solution was used as a reference cell to eliminate the effect of reflected light from the interfaces of the air/cuvette and cuvette/solution. The light transmission through Maalox-added water shows a decreasing trend with increasing Maalox concentration, but we could see fluctuations of transmission percentages due to the very short light transmission distance of the cuvette. The attenuation coefficients at 2.3 m can be calculated using the light transmission values in Fig. 8. The main purpose of Fig. 8 is to find out the overall trend of the light transmission spectra at different wavelengths through Maalox-added water. The light transmission distance of 5 mm through the Maalox solution in the cuvette is too short, and the total light attenuation is pretty low. So, the fluctuation is usually observed. Light transmission spectra measurement using a cuvette with longer light transmission distance would lead to higher accuracy of calculating the attenuation coefficient.

In addition, it is observed that the light transmission spectral peak in the green region (around 550 nm) drops at shorter and longer wavelengths. This means that blue–green light is suitable for UWOC under Maalox-added water. With higher Maalox concentration, the light attenuation shows similar increasing trends at different wavelengths, indicating similar scattering effects in water with different Maalox concentrations. In comparison, we further measured the light transmission spectra of chlorophyll solution (not shown here) and observed a strong decrease of light transmission percentage at ∼400 nm, suggesting that the absorption effect of chlorophyll solution is prominent at shorter wavelengths of ∼400 nm. Thus, in accordance with different water conditions, light sources with proper wavelengths should be carefully selected to optimize the UWOC performances.

In this Letter, we proposed and experimentally demonstrated a micro-LED-based UWOC system with light beam propagation through water with Maalox, chlorophyll, and sea salt, respectively. A blue micro-LED with a high bandwidth of hundreds of megahertz (MHz) greatly increases the transmission data rates. With tap water and different concentrations of 200.48 mg/m^3 Maalox, 12.07 mg/m^3 chlorophyll, and 5 kg/m^3 sea salt, data rates of 933, 800, 910, and 790 Mbps were achieved, respectively, with BER below the FEC threshold of 3.8×10^{-3}. We revealed mechanisms responsible for light attenuation, i.e., absorption by chlorophyll and scattering by Maalox and sea salt, and analyzed the variations of maximum data transmission rates of UWOC with concentrations of Maalox, chlorophyll, and sea salt in water. In addition, we found that the absorption effect is more sensitive to different wavelengths than the scattering effect. Our works are insightful to realize high-speed real-time UWOC in different water conditions.

This work was supported by the National Natural Science Foundation of China (NSFC) (Nos. 61705041 and 61571135), Shanghai Sailing Program (No. 17YF1429100), Shanghai Technical Standard Program (No. 18DZ2206000), State Key Laboratory of Intense Pulsed Radiation Simulation and Effect Funding (No. SKLIPR1607), and National Key Research and Development Program of China (No. 2017YFB0403603).

†These authors contributed equally to this work.

References

1. P. Tian, X. Liu, S. Yi, Y. Huang, S. Zhang, X. Zhou, L. Hu, L. Zheng, and R. Liu, Opt. Express **25**, 1193 (2017).
2. Z. Zeng, S. Fu, H. Zhang, Y. Dong, and J. Cheng, IEEE Commun. Surv. Tut. **19**, 204 (2017).
3. H. M. Oubei, R. T. ElAfandy, K. H. Park, T. K. Ng, M. S. Alouini, and B. S. Ooi, IEEE Photon. J. **9**, 7903009 (2017).
4. Y. Zhao, A. Wang, L. Zhu, W. Lv, J. Xu, S. Li, and J. Wang, Opt. Lett. **42**, 4699 (2017).
5. F. Hanson and S. Radic, Appl. Opt. **47**, 277 (2008).
6. C. Shen, Y. Guo, H. M. Oubei, T. K. Ng, G. Liu, K. H. Park, K. T. Ho, M. S. Alouini, and B. S. Ooi, Opt. Express **24**, 25502 (2016).
7. M. Kong, Y. Chen, R. Sarwar, B. Sun, Z. Xu, J. Han, J. Chen, H. Qin, and J. Xu, Opt. Express **26**, 3087 (2018).
8. X. Liu, S. Yi, X. Zhou, Z. Fang, Z. J. Qiu, L. Hu, C. Cong, L. Zheng, R. Liu, and P. Tian, Opt. Express **25**, 27937 (2017).
9. J. Xu, M. Kong, A. Lin, Y. Song, X. Yu, F. Qu, J. Han, and N. Deng, Opt. Commun. **369**, 100 (2016).
10. Y. Baykal, Appl. Opt. **55**, 8860 (2016).
11. C. Li, H. Lu, W. Tsai, Z. Wang, C. Hung, C. Su, and Y. Lu, IEEE Photonics J. **10**, 7904909 (2018).
12. X. Liu, P. Tian, Z. Wei, S. Yi, Y. Huang, X. Zhou, Z. Qiu, L. Hu, Z. Fang, C. Cong, L. Zheng, and R. Liu, IEEE Photon. J. **9**, 7204909 (2017).
13. P. Tian, Z. Wu, X. Liu, Z. Fang, S. Zhang, X. Zhou, K. Liu, M. Liu, S. Chen, C. Lee, C. Cong, L. Hu, Z. Qiu, L. Zheng, and R. Liu, Appl. Phys. Express **11**, 044101 (2018).
14. M. S. Islim, R. X. Ferreira, X. He, E. Xie, S. Videv, S. Viola, S. Watson, N. Bamiedakis, R. V. Penty, I. H. White, A. E. Kelly, E. Gu, H. Haas, and M. D. Dawson, Photon. Res. **5**, A35 (2017).
15. L. Prieur and S. Sathyendranath, Limnol. Oceanogr. **26**, 671 (1981).

16. C. Gabriel, M. A. Khalighi, S. Bourennane, P. Léon, and V. Rigaud, J. Opt. Commun. Netw. **5**, 1 (2012).
17. C. Gabriel, M. A. Khalighi, S. Bourennane, P. Leon, and V. Rigaud, in *2011 IEEE Globecom Workshops* (2011), p. 833.
18. S. K. Sahu and P. Shanmugam, Opt. Commun. **408**, 3 (2018).
19. E. Zedini, H. M. Oubei, A. Kammoun, M. Hamdi, B. S. Ooi, and M. S. Alouini, IEEE Trans. Commun. **67**, 2893 (2019).
20. A. Laux, R. Billmers, L. Mullen, B. Concannon, J. Davis, J. Prentice, and V. Contarino, J. Mod. Opt. **49**, 439 (2010).
21. X. D. Zhang, L. B. Hu, M. S. Twardowski, and J. M. Sullivan, Opt. Express **17**, 19580 (2009).
22. P. Wang, H. Chen, X. Liu, S. Yi, X. Zhou, E. Gu, K. Huang, L. Zheng, R. Liu, X. Cui, and P. Tian, in *Proceedings of 15th China International Forum on Solid State Lighting: International Forum on Wide Bandgap Semiconductors China* (2018), p. 173.
23. V. I. Haltrin, Appl. Opt. **38**, 6826 (1999).
24. M. S. Twardowski, E. Boss, J. B. Macdonald, W. S. Pegau, A. H. Barnard, and J. R. V. Zaneveld, J. Geophys. Res.: Oceans **106**, 14129 (2001).
25. Z. Gong, S. Jin, Y. Chen, J. McKendry, D. Massoubre, I. M. Watson, E. Gu, and M. D. Dawson, J. Appl. Phys. **107**, 013103 (2010).
26. P. Tian, J. J. McKendry, Z. Gong, B. Guilhabert, I. M. Watson, E. Gu, Z. Chen, G. Zhang, and M. D. Dawson, Appl. Phys. Lett. **101**, 231110 (2012).
27. F. Shen, Y. Zhou, and G. Hong, in *Advances in Computational Environment Science* (2012), p. 61.
28. L. Mullen, D. Alley, and B. Cochenour, Appl. Opt. **50**, 1396 (2011).
29. M. E. Lee and E. N. Korchemkina, *Springer Series in Light Scattering* (Springer, 2018), p. 151.
30. J. Wang, L. Liu, B. Liu, Y. Guo, Y. Zhang, R. Xu, S. Wang, and X. Zhang, Spectrochim. Acta A Mol. Biomol. Spectrosc. **75**, 366 (2010).